ELSEVIER

International Journal of Mass Spectrometry 185/186/187 (1999) 773–786

International Journal of Mass Spectrometry

Thermally activated decay channels of superhot C_{60}^-: delayed electron emission and dissociative attachment studied by hyperthermal negative surface ionization

A. Bekkerman, B. Tsipinyuk, E. Kolodney*

Department of Chemistry, Technion—Israel Institute of Chemistry, Haifa 32000, Israel

Received 10 July 1998; accepted 19 September 1998

Abstract

Superhot C_{60}^- ions were formed by attachment of low energy free electrons to superhot C_{60}^0 molecules in effusive beam. We have studied the thermally activated decay of the C_{60}^- ion as a function of its vibrational temperature. In addition to the main channel of delayed electron emission $C_{60}^- \rightarrow C_{60}^0 + e^-$, we give evidence for a secondary channel (only weakly competitive) of dissociative attachment $C_{60}^0 + e^- \rightarrow C_{58}^0 + C_2^-$. We have found no evidence for the nearly isoenergetic complementary channel $C_{60}^0 + e^- \rightarrow C_{58}^- + C_2^0$. In order to measure the initial C_{60}^- beam flux (which partially decays to C_{60}^0 during the flight time) independently for each nozzle temperature we have used a unique detection method that is completely insensitive to the initial charge state and therefore to the ratio of charge states in the primary beam. The method is based on collisional electron exchange and negative ion (C_{60}^-) formation in a hyperthermal collision with a surface. Analyzing the kinetics of the delayed electron emission we have obtained a straight Arrhenius plot with a slope (activation energy) of 2.64 ± 0.07 eV and intersection (A value) of 1.3×10^{11} s^{-1}. This value of the pre-exponential factor is in good agreement with former measurements but is several orders of magnitude lower than current models' predictions. A possible explanation for this difference is discussed. (Int J Mass Spectrom 185/186/187 (1999) 773–786) © 1999 Elsevier Science B.V.

Keywords: Fullerenes; Electron emission; Surface ionization; Metastable negative ions; Dissociative attachment

1. Introduction

Recently there has been an increased interest in studying the decay dynamics of long lived metastable negative ions including large molecular ions and clusters [1–3]. The two main processes observed under collision-free conditions are delayed auto-detachment (AD) of electrons and delayed dissociative electron attachment (DA). The dissociative channel leads to the formation of negatively charged fragment ion. The C_{60}^- negative ion has attracted attention with regard to its formation via free electron capture and delayed electron detachment kinetics [4–11] (that could alternatively be described as thermionic emission). We have recently provided direct experimental evidence for the thermal nature of delayed electron emission from a superhot (highly vibrationally excited) neutral C_{60}^0 molecule [12] on the time scale of hundreds of microseconds. For C_{60}^-, it was already shown that the electron detachment kinetics behaves

* Corresponding author.

Dedicated to Professor Michael T. Bowers on the occasion of his 60th birthday.

1387-3806/99/$20.00 © 1999 Elsevier Science B.V. All rights reserved
PII S1387-3806(98)14194-5

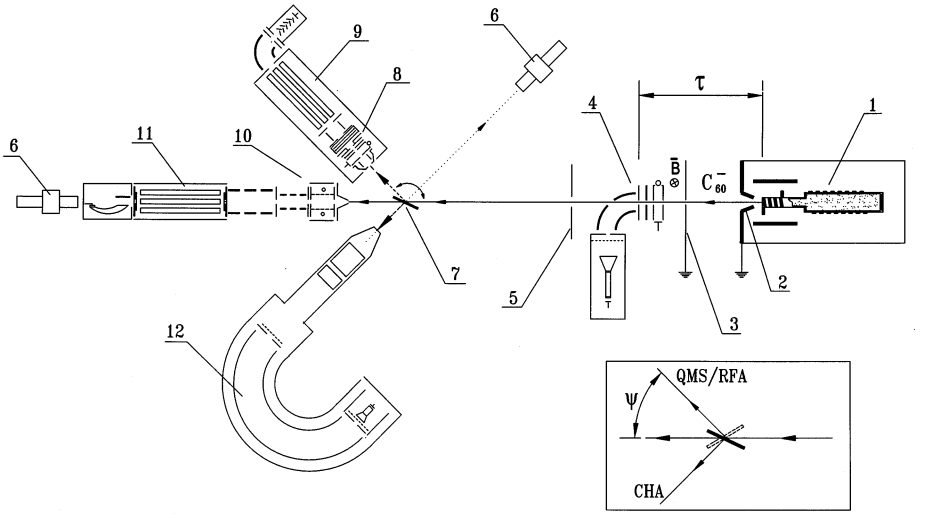

Fig. 1. The experimental setup: (1) Two stage all ceramic beam source, (2) ion extractor, (3) beam defining aperture, (4) 90° electrostatic energy analyzer/deflector, (5) beam defining aperture, (6) micro-optical pyrometer, (7) rotatable surface, (8) retarding field analyzer, (9) quadrupole mass filter (Balzers QMG-421), (10) ion transfer optics, (11) quadrupole mass filter (Extrel MEXM-4000), (12) hemispherical energy analyzer (CHA VG-100AX). Insert: a schematic view of the scattering geometry.

thermally following nonthermal but well-defined energy pumping by attaching kinetic energy resolved electrons [5,6,11]. The activation energy obtained was in good agreement with the reported electron affinity (EA = 2.65 eV) value of C_{60} [13] but the pre-exponential factor was orders of magnitude lower than predicted by simple models [14,15]. No dissociative attachment channel was observed [5]. In this article we will describe our study of the decay dynamics of thermally excited C_{60}^-. The issues addressed are: (1) How well does thermal kinetics (Arrhenius plots) describe the delayed electron emission of a thermally pumped (initially canonical at the oven aperture) ensemble of C_{60}^- ions? (2) Can one observe, under thermal excitation conditions, a competitive dissociative electron attachment channel leading to the delayed formation of C_2^- or C_{58}^-? (3) The two possible DA processes: $C_{60}^- \rightarrow C_{58}^- + C_2^0$ and $C_{60}^- \rightarrow C_{58}^0 + C_2^-$ are of nearly equal endothermicity ($EA(C_2)$ = 3.27 eV [16] whereas $EA(C_{58}) = 3.3 \pm 0.1$ eV [17]). If these two processes are observable, what will be the branching ratio between them? (4) For extracting the rate constants of electron detachment from C_{60}^- we are using a different method than previously employed [6,11]. If indeed thermal behaviour is obeyed, our new approach will provide an additional independent way to determine the pre-exponential factor, a value that may be an important input for future theoretical treatments.

Finally, in recent years C_{60} has become a model system for studies of decay processes in highly energized isolated microscopic particles like large molecules or tightly bound clusters. We have focused on studying thermally activated processes of an ensemble (initially canonical) of isolated superhot C_{60} molecules or ions. The measurements presented here are an additional step in this direction.

2. Experimental setup and methodology

The experimental setup is presented in Fig. 1. A two-stage, all-ceramic nozzle oven assembly is the source for a C_{60}^0 effusive beam. This is a constant flux source, independent of the nozzle temperature T. A detailed description of the beam source was given before [18,19]. Briefly, the temperature of the C_{60}^0 vapours at the first stage (the evaporator) is around 1000 K and the temperature of the C_{60}^0 molecules exiting the nozzle aperture can be independently

varied in the range of $T = 1000–2000$ K (roughly corresponding to an average vibrational energy of 7–20 eV). Temperature of the second (nozzle) stage is achieved using resistive heating with a thin rhenium ribbon that at the same time is also the source for low kinetic energy ($\langle E_e \rangle$) electrons for soft attachment to the neutral C_{60} effusive beam. An experimental measurement of $\langle E_e \rangle$ will be described in Sec. 3.2. Special emphasis was given to accurate measurement (± 3 K) of relative changes in nozzle temperature (temperature differentials). This is because of the fact that the analysis of the experimental results is in terms of temperature differences (which can be more accurately determined) rather than absolute temperature values. Temperatures were measured by a micro-optical pyrometer situated either on the beam axis or at an angle of 45° to the beam axis using specular reflection from a polished (mirror-like) Si(100) surface. The whole system was independently calibrated by accurate temperature measurements of hot rhenium foil mounted instead of the nozzle front face with and without the ion optics apertures and beam defining elements.

In the case where the beam source provides a constant flux of C_{60}^- over all of the relevant temperature range one can extract thermal characteristics just by following the attenuation of the C_{60}^- flux or increase of the C_{60}^0 signal during a given flight time as a function of the nozzle temperature T (converted into vibrational temperature). The primary C_{60}^- flux (without decay) can be measured at some low reference temperature. Our nozzle is a constant flux source for the primary C_{60}^0 beam (just emerging from the nozzle aperture) [19,20] but the coupling between the temperature of the heating filament and the electron density at the attachment region preclude the possibility of an a priory assumption of a constant C_{60}^- flux. In former reported measurements [6,11], rate constants for C_{60}^- decay as a function of internal energy were measured by controlling the ion kinetic energies (i.e. flight times) inside the mass spectrometer. This procedure is valid as long as there is no coupling between the ion energy and the instrumental transmission function or initial flux. We have adopted a different approach based on monitoring the increase of the C_{60}^0 signal while normalizing for the initial C_{60}^- flux separately and independently for each nozzle temperature. This approach is the one best suited for our experimental configuration. Moreover, the flux normalization method presented here is unique and interesting in itself and provides an important application of hyperthermal surface ionization (total flux normalization that is independent of the incident charge fractions). We believe that this method is of general importance in similar situations. In the following we will describe the experimental procedure and the flux normalization method.

C_{60}^- ions are extracted from the electron attachment region and electrostatically accelerated to a final kinetic energy $E_0 = 100$ eV. It was verified that free electrons are not extracted into the field free region. The thermal decay of the superhot C_{60}^- ions takes place during the flight time $\tau = 42.5 \pm 1$ μs (as is defined in Fig. 1) along the field free path up to the entrance aperture of the analyzer. Both C_{60}^0 (formed during τ) and C_{60}^- (that survived past τ) reach the 90° electrostatic deflector/energy analyzer (#4 in Fig. 1). The C_{60}^- ions can now be deflected off the beam axis leaving only the neutral C_{60}^0 to be detected downstream. If the deflection potential is not applied, the nondepleted beam (comprised of both C_{60}^0 and C_{60}^-) will continue without interruption towards the detector. The analyzer is also equipped with an ionizer in order to verify $E_0 = 100$ eV for both neutrals (electron impact ionized) and negative ions (ionizer on/off and reversing all polarities as needed). Mass analysis of the primary beams was carried out using an Extrel MEXM-4000 quadrupole mass spectrometer (QMS) that was mounted on the beam line (#10,11 in Fig. 1). As mentioned before, our measurement method is based on independent normalization over the C_{60}^- initial flux for each nozzle temperature. Because a fraction of the C_{60}^- decays into C_{60}^0 during the beam flight time to the detector, one gets a mixture of charge states with unknown ratio. The required normalization method should therefore be one that does not discriminate between the different charge states. Common ionization based detection methods usually employed in mass spectrometry are inappropriate. However, a detection method that does fulfill this requirement was recently studied by us and is based on charge ex-

change and negative ion formation in hyperthermal collisions of fullerenes with surfaces [21].

We have recently found that neutral C_{60}^0, aerodynamically accelerated in seeded beams to hyperthermal energies of $E_0 = 10–50$ eV, is scattered off a monolayer graphite on nickel (Ni/C) as a negative ion with high efficiency [21]. The negative ion formation yield strongly increases with E_0 and approaches 1% of the incoming neutral flux for the highest E_0. Up to a normal impact energy of $E_{0\perp} = 32$ eV the scattered negative ion spectrum is totally dominated by the C_{60}^- molecular peak. There are no fragments observed down to a level below 10^{-4} of the scattered C_{60}^- intensity [21]. The phenomena itself for neutral polyatomic molecules in the incidence energy range $E_0 = 1–10$ eV was observed and reported before and was named negative hyperthermal surface ionization [22,23]. The charge exchange process and negative ion formation in a low velocity collision with a surface is completely insensitive to the incoming charge [24]. The incident particle loses track of its initial charge state at some critical distance from the surface. Starting from this critical distance there is a mixing between the particle electrons and the target conduction electrons (via resonance exchange). The final charge fractions are therefore exclusively determined along the outgoing trajectory irrespective of the incident charge [24]. This argument is fully justified for atomic collisions and nondissociative molecular collisions at low normal velocities ($V_{0\perp} = 10^{-3}$–10^{-2} a.u.) as is the case here. However, as a general comment, it should be noted that in the case of dissociative scattering of molecular positive ions from surfaces it is possible that, due to electron transfer to a repulsive electronic (dissociative neutralization) state, the ratio of scattered fragments will depend on the initial charge state [25]. Under our experimental conditions ($E_{0\perp} = 18$ eV), molecular vibrational excitation of C_{60}^0 upon surface impact is negligible [26,27] and there is no collisional dissociation of C_{60}^0 down to a level below 10^{-4} of the scattered C_{60}^- intensity. All the scattering experiments reported here were carried out with the graphite on nickel (Ni/C) surface at a scattering angle of $\psi = 45°$ (near grazing geometry with incidence angle 65°). A detailed account of surface preparation and scattering conditions is given elsewhere [28,30]. Base pressure at the scattering chamber is 5×10^{-10} Torr. The mirror-like silicon surface used for the pyrometric measurement is mounted on top of the Ni/C surface (along the manipulator axis), in a double sample holder. In this study we measure the scattered C_{60}^- intensity with and without deflection. When deflection voltage is applied, only C_{60}^0 molecules (that are formed by autodetachment during τ) hit the surface. Without the deflection voltage the full nondepleted flux ($C_{60}^0 + C_{60}^-$) hits the surface. This flux is proportional to the initial C_{60}^- flux at the point of ion formation near the nozzle aperture. The collisionally formed C_{60}^- can then be detected at $\psi = 45°$ by a quadrupole mass spectrometer (Balzers QMG-421) equipped with a home-made retarding field analyzer (RFA) or by a hemispherical energy analyzer (VG-100AX). Both scattering configurations are equivalent. For measuring the scattered C_{60}^- flux we used mainly the hemispherical analyzer. Since the C_{60}^- signal constituted more than 98% of the scattered intensity, mass separation was not required. About 2% of the total negative ion signal was C_{58}^-, which could be neglected for the decay analysis, as will be discussed in Sec. 3.2.

Fig. 2(a) shows energy distributions of scattered C_{60}^- for primary beam incidence with $E_0 = 100$ eV and nozzle temperature $T = 1620$ K, with and without deflection. Under "deflector ON" conditions only C_{60}^0 is left in the beam (after flight time τ) and hits the surface (solid circles). Under "deflector OFF" conditions, the full nondepleted beam ($C_{60}^0 + C_{60}^-$) hits the surface (empty circles). The scattered C_{60}^- integrated intensities ratio between these two primary beam conditions (as a function of nozzle temperature) constitute the basic measurement for the decay analysis. The scattering dynamics for these two primary beam conditions is practically the same, as is evidenced by the similarity of their energy and angular distributions. Fig. 2(b) shows superposition of the two spectra of Fig. 2(a), but is normalized to the same maximum intensity. The perfect overlap of the two spectra demonstrates the insensitivity to the initial charge state. The behaviour presented in Fig. 2 for $T = 1620$ K is observed over all the nozzle temper-

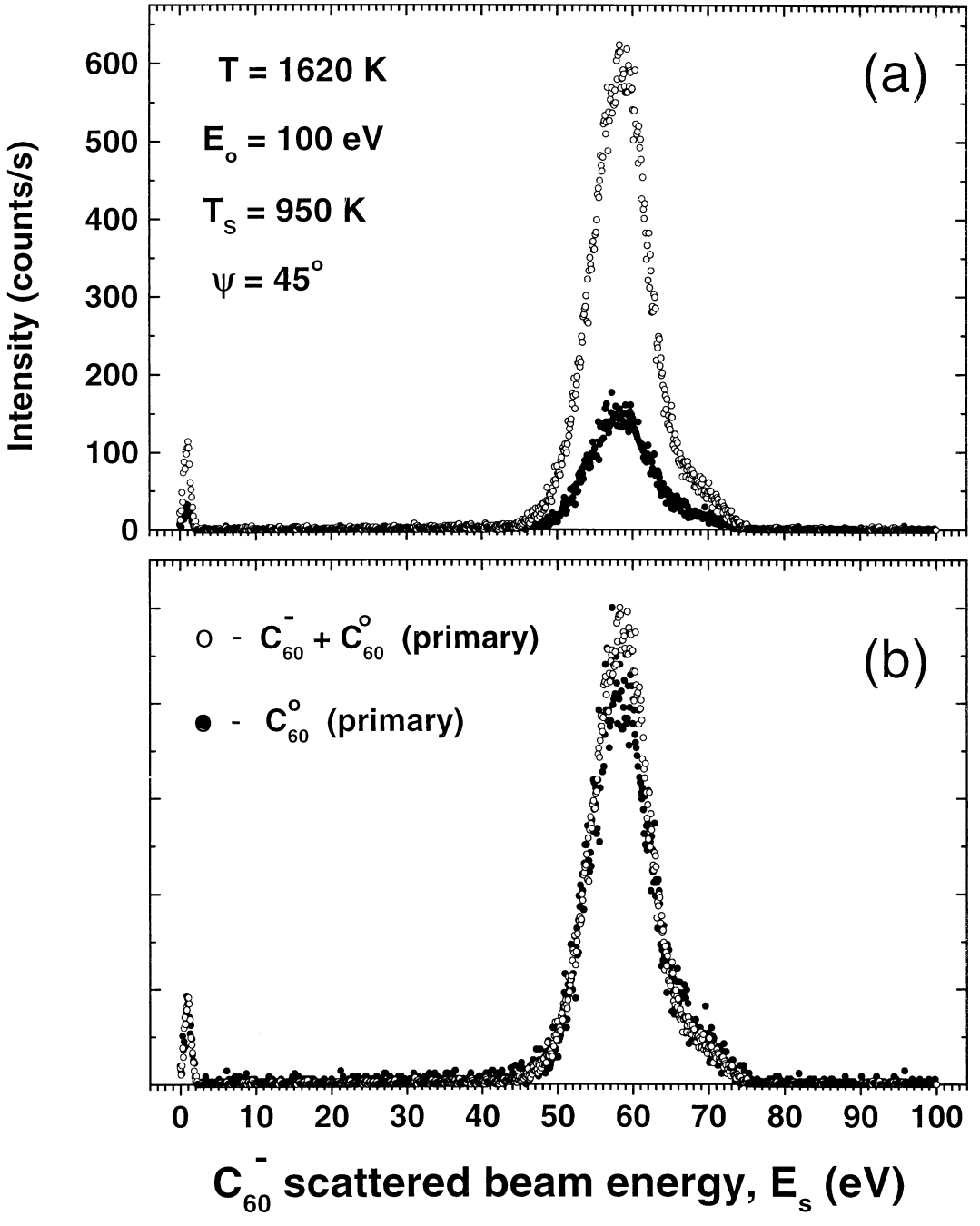

Fig. 2. (a) Energy distributions of scattered C_{60}^- following impact of primary beams (E_0 = 100 eV, T = 1620 K) with different charge state compositions. The empty circles are for the nondepleted primary beam (C_{60}^- + C_{60}^0, deflector off) and the solid circles are for the C_{60}^0 only beam (deflector on). The ratio of the scattered C_{60}^- intensities as shown here (measured with the hemispherical analyzer) constitutes the basic data point (α) in this flux calibrated measurement. The peak near zero energy is due to thermal electrons detached from the scattered C_{60}^- along its flight time from the surface to the hemispherical analyzer; (b) same as (a) but with both spectra normalized to the same maximum intensity. Note the complete overlap of the two scattered C_{60}^- energy distributions, demonstrating insensitivity to the initial charge state. The similar scaling observed for the auto-detached electrons peak show that both scattered C_{60}^- beams have the same vibrational temperature.

ature range studied here. Similarly, perfect overlap is also found between scattered C_{60}^- angular distributions for the two scattering conditions. Indeed, incidence angle dependences (under the experimental configuration of constant scattering angle) are sharp and symmetric without any background contributions, and with full width at half maximum (FWHM) of 7°. The effective entrance aperture of the hemispherical analyzer in the scattering plane (including the ion optics elements) is about 12°. We therefore fully integrate over the scattered C_{60}^- angle distributions. All the experimental results reported here are also reproduced when using the QMS/RFA whose effective entrance aperture is 3°. The insensitivity to the angular width of the entrance aperture (with respect to the width of the angular distribution) is a direct result of the similarity of the scattered C_{60}^- angular distribution for the two primary beam conditions.

Besides their initial charge states, the incoming C_{60}^- and C_{60}^0 differ also in their vibrational temperatures. Being a decay product of C_{60}^-, the neutral C_{60}^0 is colder than the parent C_{60}^- by $EA(C_{60}) = 2.65$ eV. This difference in vibrational excitation between the two charge states can have, in principle, some influence on both the formation yield of C_{60}^- upon surface impact and its decay (via electron emission) after scattering (on the way to the detector). The overlapping spectra as presented in Fig. 2(b) provide us with experimental evidence that the two charge states are also indistinguishable with regard to their vibrational energies upon impact. The peak near zero energy is attributed to delayed thermal electrons that detached from the scattered C_{60}^- along its way to the detector. The fact that the intensity of these delayed electrons is proportional to the scattered C_{60}^- intensity irrespective of the charge states composition of the primary beam (with or without the hotter C_{60}^-) is a clear indication that under the present experimental conditions (initial vibrational energies of 15–19 eV) the scattered C_{60}^- signal is insensitive to the relatively small difference in vibrational energies between the two charge states. It seems that the most plausible explanation for this insensitivity to the initial vibrational excitation can be given in terms of an effect already reported and analyzed by us for the same collider/surface system [27]. In the scattering of hyperthermal neutral C_{60}^0 off Ni/C we have observed an inverse dependence of the impact induced vibrational excitation on the initial vibrational energy of the incident fullerene [27]: the higher the vibrational excitation of the incoming C_{60}^0, the lower the probability for vibrational excitation upon impact. This effect was rationalized by us in terms of two counter-balancing effects: deformation induced excitation (heating) and partial thermal accommodation with the colder surface (cooling). As a direct result of this effect, all the scattered C_{60}^- ions leave the surface with nearly the same vibrational temperature, in spite of the difference in the vibrational temperatures of the incoming C_{60}^0 and C_{60}^-.

3. Results and analysis

3.1. The C_{60}^- decay channels: auto-detachment (AD) and delayed dissociative attachment (DA)

The decay channels of superhot C_{60}^- that will be considered here are delayed electron emission (AD) and two complementary delayed fragmentation (DA) channels, according to the following scheme:

$$C_{60}^- \rightarrow C_{60}^0 + e^- \quad (1a)$$

$$\rightarrow C_{58}^0 + C_2^- \quad (1b)$$

$$\rightarrow C_{58}^- + C_2^0 \quad (1c)$$

The dissociation energy E_d of C_{60}^0 is still a matter of controversy. A value of 7–8 eV was reported based on mass spectrometric analysis of the dissociation products of electron impact excited C_{60}^+ [29]. The dissociation energy of purely thermally excited (superhot) C_{60}^0 into $C_{58}^0 + C_2^0$ was measured by us using several independent methods [12,18–20,31] and was consistently found to be in the range of $E_d = 4.2$–4.8 eV. We will therefore assume an average value of 4.5 eV. The most recent and accurate measurement for the electron affinity of dicarbon C_2 yielded the value [16] $EA(C_2) = 3.269 \pm 0.006$ eV using photoelectron spectroscopy. Former measurements [32] gave a value of 3.39 ± 0.02 eV. The electron affinity of C_{58} was measured [17] by photodetachment (UV

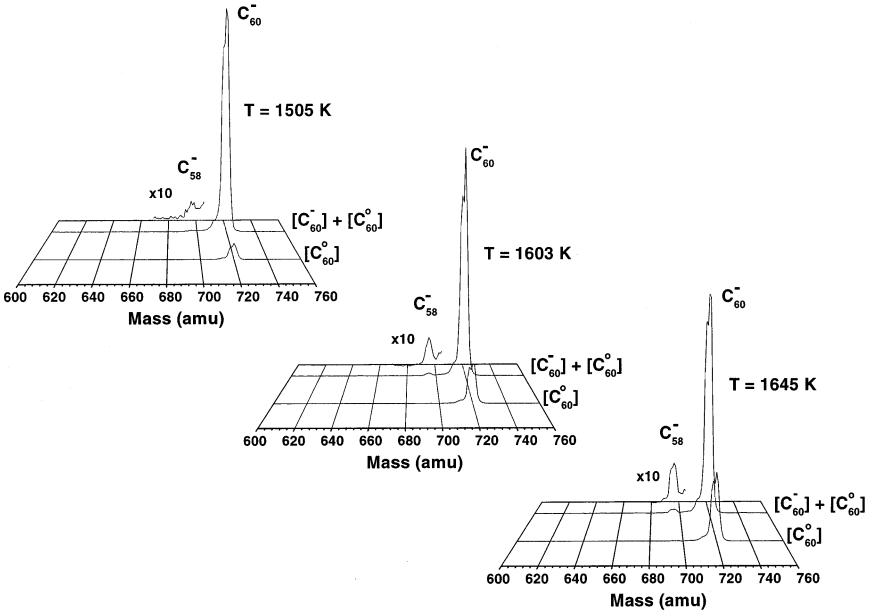

Fig. 3. Surface scattered negative ion mass spectra following $E_0 = 100$ eV primary beam impact with different nozzle temperatures. For each temperature two different spectra are shown: one for the nondepleted primary beam including both charge states ($C_{60}^- + C_{60}^0$) and the second one for pure C_{60}^0 beam (after deflection of the C_{60}^- ions). Because collisional dissociation at this normal energy ($E_{0\perp} = 18$ eV) is below the 10^{-4} level of the C_{60}^- signal intensity the spectra reflects the relative abundance of the incident beam species (ions or neutrals) just before surface impact. Note the gradual rise of the C_{58}^- signal.

photoelectron spectroscopy) as $EA(C_{58}) = 3.3 \pm 0.1$ eV. The same group has carried out extensive measurements of electron photodetachment energies from carbon clusters anions [33] and also measured $EA(C_2) = 3.3 \pm 0.1$ eV, in good agreement with the more accurate results. Because no geometry change (relative shift of potential curve) is expected during transition from C_{58}^- to C_{58}^0 one can safely assume that the vertical detachment energy measured is very close to the adiabatic electron affinity. Using these energies we can calculate the ΔH value for the different decay channels. For the delayed electron emission channel we obviously have ΔH (1a) $= EA(C_{60}) = 2.65$ eV. For the (1b) channel we get ΔH (1b) $= E_d + EA(C_{60}) - EA(C_2) = 3.85$ eV and for the (1c) channel $\Delta H(1c) = E_d + EA(C_{60}) - EA(C_{58}) = 3.85$ eV. From the energetics of the different channels it is clear that: (1) The DA channels are only very weakly competitive with the AD channel, and because of the very similar EA values of C_2 and C_{58} the two complementary DA channels are nearly isoenergetic. The excess electron ground state wave function of the parent C_{60}^- ion is spherically symmetrically spread over the carbon cage. This practically equal endothermicity combined with the high symmetry of the excess electron wave function presents an intriguing situation. Based on energy consideration alone, in the fully adiabatic limit (very slow process) one should expect a 1:1 branching ratio.

Fig. 3 shows mass spectra of surface scattered negative ions following impact of $E_0 = 100$ eV ($E_{0\perp} = 18$ eV) primary beams for three different nozzle temperatures. For each temperature the two spectra shown correspond to nondepleted ($C_{60}^- + C_{60}^0$) and depleted (C_{60}^0 only, after deflection of C_{60}^-) primary beams. The two most prominent features in Fig. 3 are the gradual increase of the C_{60}^0 concentration (in the primary beam) and the observation of scattered C_{58}^- and its temperature dependence. The scattered C_{58}^- was observed for both the nondepleted and depleted primary beams. However, it was much weaker for the depleted beam (C_{60}^0 only) and for

clarity of presentation was not magnified in Fig. 3. The intensities ratio of scattered C_{58}^-/C_{60}^- for any of the three T values in Fig. 3 is four times smaller for the depleted beam than for the undepleted one. Both scattered C_{60}^- and C_{58}^- have high kinetic energy (around 60 eV) as is shown in Fig. 2 for C_{60}^-. Furthermore, the mass spectrum in Fig. 3 is energy gated at 60 ± 20 eV. This clearly shows that the origin of the scattered C_{58}^- is either from the 100 eV C_{60}^- primary beam or from C_{58}^- (in the primary beam) that was formed independently near the nozzle and thus have the same E_0.

The scattered C_{58}^- signal is not due to collision induced dissociation (CID). The evidence for this is as follows: (1) In the study reported here $E_{0\perp} = 18$ eV and the scattering dynamics (energy losses, see Fig. 2) is exactly the same as for the former neutral C_{60}^0 ($E_0 = 10$–50 eV) seeded beam experiments [30]. Negative ions mass spectrum following the scattering of seeded beam C_{60}^0 with $E_{0\perp}$ up to 32 eV have shown the absence of collision induced C_{58}^- down to a level below 10^{-4} of the scattered C_{60}^- [21]. This observation rules out the possibility of impulsive collision induced formation of C_{58}^0 (at the surface) followed by immediate electron pickup to form C_{58}^-. It also shows that under these conditions the scattered C_{60}^- does not decay into C_{58}^- via channel (1c). (2) C_{60}^0 and C_{60}^- in the primary beam here are hotter (by about 2–4 eV) than the seeded beam C_{60}^0. One may argue that the delayed DA channel (1c), although not observed for the slightly colder seeded beam C_{60}^0, may result here from the decay of collisionally (vibrationally) excited C_{60}^- on its way from the surface to the detector. However, measured vibrational excitation under similar conditions (both $E_{0\perp}$ and initial vibrational energy) was found to be negligible, namely less than 1 eV, especially for high initial vibrational energies [26,27] (see also the discussion in Sec. 2 regarding the insensitivity to a few electronvolts difference in initial vibrational energies). We thus conclude that the spectra in Fig. 3 reflect the mass abundance (either neutral or ionic species) in the primary beam at the instant of surface impact. We note that the strong disproportionality observed between the scattered C_{58}^- and C_{60}^- intensities for the depleted and nondepleted beams (Fig. 3) is also not in accordance with the possibility of CID as the origin for C_{58}^-. It can be rationalized based on discrimination effects (due to dissociative recoil, as will be discussed later) related to the point of formation along the flight path of either C_{58}^0 or C_{58}^- in the primary beam. Fig. 3 also provides us with information regarding the relative importance of the AD channel as compared with the DA channels. Since $EA(C_{58}) > EA(C_{60})$ the yield of the scattered C_{58}^- via surface electron pickup (resonance tunneling) should be much higher than the yield of C_{60}^-. (This bias in favour of C_{58}^- is partially compensated for by solid angle discrimination against C_{58}^- as will be discussed later). As a result, one can conclude that the C_{60}^0 concentration in the primary beam is higher by at least a factor of 100 than the C_{58}^0 or C_{58}^- concentration. This is seen by comparing scattered C_{60}^- and C_{58}^- signal intensities independently for each primary beam. It is obvious that the electron emission channel (1a) is the dominant one and therefore we can safely analyze the thermal kinetics of the AD channel while neglecting the DA channels. As already mentioned with regard to Fig. 2, the intensities ratio of the scattered C_{60}^- for the two primary beam conditions (C_{60}^0 only versus $C_{60}^0 + C_{60}^-$) is the basic measurement and reflects the decay kinetics. A detailed description of the analysis will be given in the next section.

So far we have shown that the source of the scattered C_{58}^- must be high energy ($\sim$100 eV) C_{58}^0 or C_{58}^- in the primary beam. Formation of C_{58}^0 from consecutive fragmentation of the product C_{60}^0 in (1a) can be ruled out since we know that the C_{60}^0 in this case is colder by 2.65 eV than C_{60}^-. At this stage we cannot yet distinguish between the two complementary DA channels and we still need to verify that no C_{58}^- is formed from C_{58}^0 between the nozzle and the extractor cone. In order to further investigate the source of the C_{58} (neutral or ion) we have measured the negative ion mass spectrum of the primary beam as shown in Fig. 4 (for nozzle temperature of 1645 K). No fragments were found down to the detection limit, which for C_{58}^- was below 1×10^{-4} of the C_{60}^- signal intensity. This observation rules out all the possible processes that can lead to formation of C_{58}^- in the primary beam including: (1) the formation of C_{58}^- via

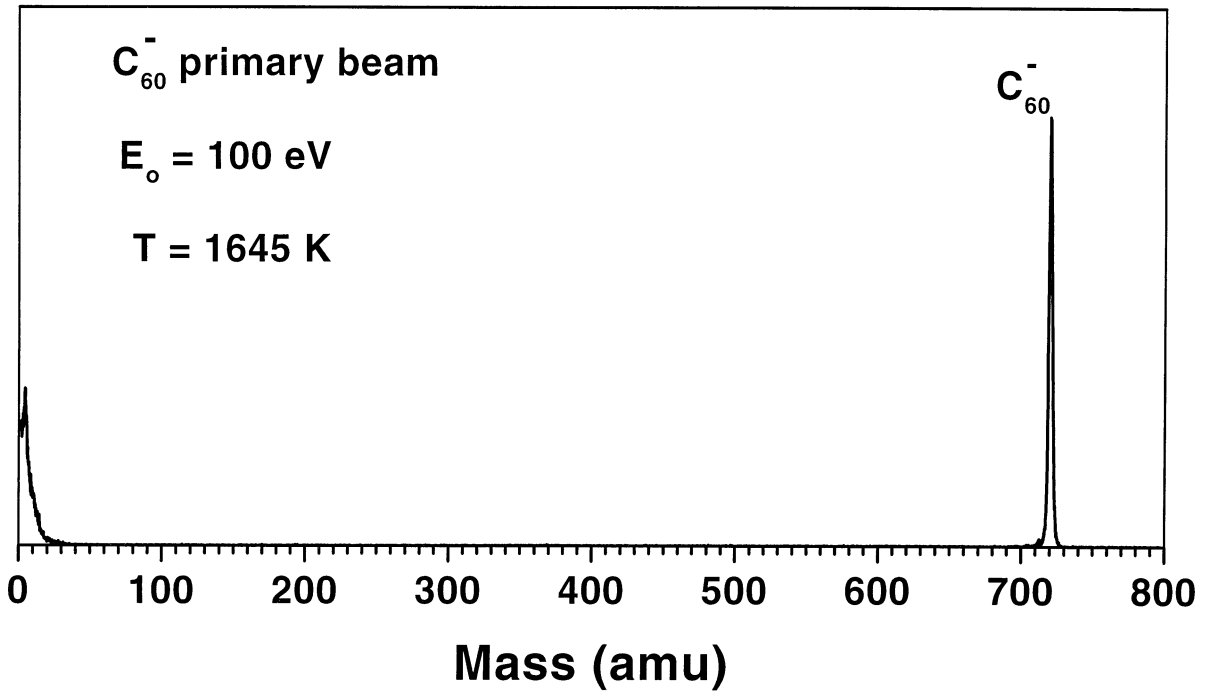

Fig. 4. Negative ion mass spectra of the primary beam (E_0 = 100 eV) as measured along the beam axis by the on-line QMS (#1 in Fig. 1). There is no C_{58}^- signal down to the detection limit of 1×10^{-4} of the C_{60}^- intensity (reduced sensitivity because of the high ion energy). The low mass peak originates from C_{60}^- but is a QMS artefact that was broadened because of the high ion energy (>100 eV) and low resolution conditions for the low masses (optimized conditions only for the high mass range).

C_{60}^0 fragmentation to C_{58}^0 in the nozzle throat followed by electron capture, and (2) the prompt or delayed DA channel (1c). Two comments are in order regarding possible discriminating effects between C_{58} and C_{60} (neutrals or ions) involved in the last two processes. First, the gas phase electron capture cross section (free molecule–free electron) is usually not correlated with the molecular EA value. Because ionic diameters of C_{58}^- and C_{60}^- are probably very close it is reasonable to assume similar attachment cross sections; namely no discrimination with regard to the negative ion formation is expected. Second, the kinetic energy release distribution (KERD) for the (1c) and (1b) fragmentation processes peaks at 0.2 eV [34,35] and extends up to 0.4–0.5 eV. Taking into account the angular width of the primary beam entering the mass spectrometer and the divergence due to recoil along the beam flight time, we have calculated that about half of the C_{58}^0 (or C_{58}^-) formed is detected. This minor solid angle discrimination against the C_{58} species does not change our conclusion. Unfortunately, the recoil effect is much more pronounced for the C_2^0 (or C_2^-) fragments that carry only 0.033 E_0 (3.3 eV) and are therefore strongly spatially discriminated against and cannot be used for monitoring the DA channels. The spectrum presented in Fig. 4 is optimized for high masses (resulting in low mass artefact). We have also optimized the QMS scanning conditions for the low mass region but no C_2^- was detected.

We believe that the experimental evidence presented here eliminates all possible sources for the scattered C_{58}^-, thus leaving channel (1b) as the only possible option. We conclude that this DA channel is dominant over the complementary process (1c). The hyperthermal negative surface ionization is simply a much more sensitive way for detecting high energy neutral C_{58}^0 formed in the beam as compared with electron impact ionization based detection that could not generate enough signal (especially at high E_0). Finally, one can also show that the measured C_{58}^-/C_{60}^-

intensities ratio is compatible with the ΔH value derived for the DA (1b) decay channel. Using the scattered C_{58}^- and C_{60}^- intensities as in Fig. 3 and correcting for the differences in electron affinities between C_{58}^0 and C_{60}^0 (assuming that the scattered C_{58}^- formation yield is up to a factor of 10 higher than that of C_{60}^-) and the recoil based discrimination factor, we roughly estimate the ratio of $[C_{60}^0]/[C_{58}^0]$ in the primary beam [products of (1a) and (1b)] to be 100–300. If the efficiency for surface electron pickup by the hyperthermal C_{58}^0 is higher than that of C_{60}^0 by more than a factor 10 the C_{58}^0 abundance in the primary beam will be below 0.3%. For two parallel first order reactions the products concentration ratio is simply given by the ratio of the corresponding rate constants. The estimated concentrations ratio agrees well with the calculated ratio of thermal (Arrhenius type) rate constants between channels (1a) and (1b) using the given ΔH values and within some reasonable limits for the ratio of pre-exponential factors. Based on measured pre-exponential factors for the AD channel (2.5×10^{11} s^{-1} [6] and in this study 1.3×10^{11} s^{-1}) and for C_{60}^0 and C_{60}^+ fragmentation (2.5×10^{13} s^{-1} [18,31]) we have assumed a ratio of pre-exponential factors between 3 and 10 in favour of channel (1b). In formerly reported measurements [6] where the C_{60}^- was nonthermally pumped by the attached electrons, the DA channel (1b) leading to C_{58}^0 was not observed and the complementary channel (1c) leading to C_{58}^- was not considered.

We will now discuss possible explanations for the experimentally observed branching ratio between the two DA channels. As already mentioned, based on the nearly equal endothermicity, the expected branching ratio should be 1:1. Moreover, on top of the purely energetic reasoning and based on statistical dilution considerations for the departing electron one might predict some preference for electron localization on the C_{58} fragment. This way, the electron will be sampling a much larger part of the available phase space initially occupied by the C_{60}^- excess electron. According to these arguments, one would expect the branching ratio to be in favour of channel (1c). This conclusion is clearly in contrast with the experimental observation. A situation that does obey this type of reasoning was reported for dissociation of a C_6F_5I negative ion [1]. Although the EA values of C_6F_5 and I were reported to be very close, the observed branching ratio was 1:10 in favour of $C_6F_5^-$. In this case the electron clearly preferred localization on the larger polyatomic fragment. At the moment, the only explanation we can provide for the unexpected dominance of channel (1b) is that the emission of the C_2 unit from the C_{60} skeleton is a very slow process and therefore fully adiabatic. The excess electron thus completely adjusts to the nuclear motion. In this case even a small difference of 0.1–0.2 eV (within experimental uncertainty) between EA(C_{58}) and EA(C_2) values in favour of C_2 will lead to electron localization on the C_2 fragment. We note that the relatively low pre-exponential factor measured for C_2 emission from C_{60}^0 and C_{60}^+ [18,30] supports this interpretation.

3.2. Thermal decay analysis of the auto-detachment channel

In Sec. 3.1 we showed that the auto-detachment channel strongly dominates over all other channels. The decay kinetics of superhot C_{60}^- can therefore be analyzed as a first order electron emission process as reported before [6,11]. Fig. 5 shows the dependence of the fraction

$$\alpha = \frac{\text{scattered } [C_{60}^-]\text{: “deflector ON”}}{\text{scattered } [C_{60}^-]\text{: “deflector OFF”}}$$

on nozzle temperatures in the range of 1450–1620 K. These measurements contain all the information on the thermal decay kinetics of C_{60}^- during the flight time τ. In the following we will analyse these results.

Let I_0 be the primary C_{60}^- beam flux (at the ion formation point) with an average internal energy per molecule:

$$E_V = \langle E_{\text{th}}(T) \rangle + \text{EA} + \langle E_e \rangle \quad (2)$$

where $\langle E_{\text{th}}(T) \rangle$ is the intramolecular canonical energy (thermal) for a nozzle temperature T and $\langle E_e \rangle$ is the average kinetic energy carried by the captured electron. Here we have assumed that the energies EA + $\langle E_e \rangle$ are redistributed among all the molecular vibra-

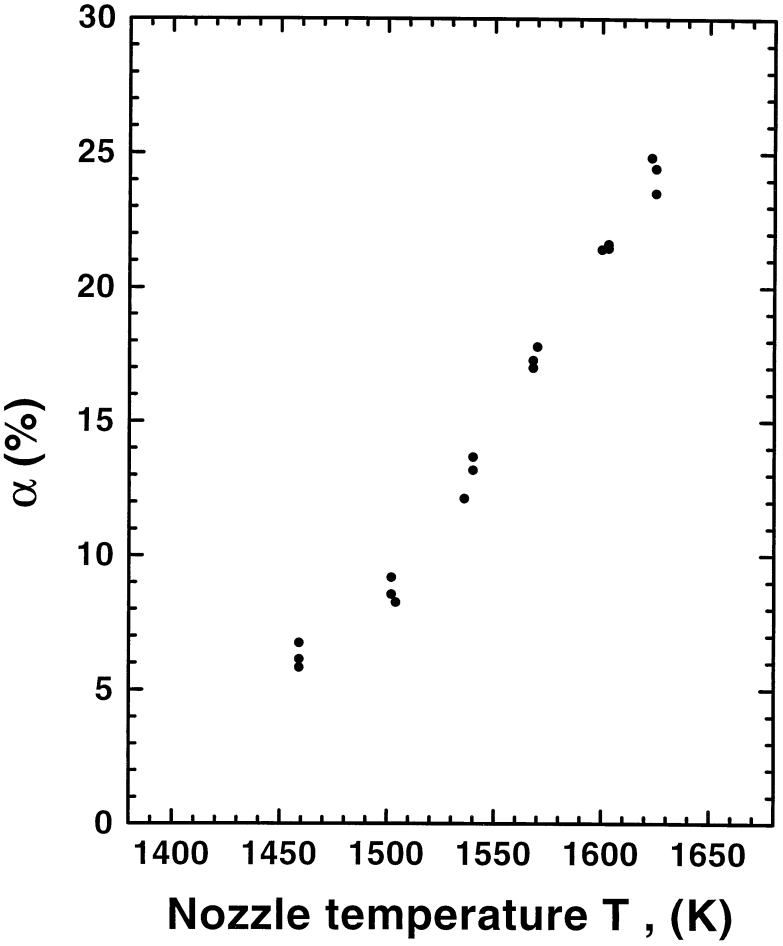

Fig. 5. Nozzle temperature dependence of the fraction α = (scattered [C_{60}^-]: "deflector ON"/(scattered [C_{60}^-]: "deflector OFF") due to auto-detachment of electrons from C_{60}^- along the flight time τ (as defined in Fig. 1). The three sets of independent measurements shown reflect the reproducibility of the experimental results.

tions on a time scale much shorter than the flight time. E_V is related to a vibrational temperature T_V via the approximated relation E_V (eV) = 13.9 + 0.0143(T_V(K) − 1500) for 4000 K > T_V > 1500 K [26]. Along their flight path towards the target, C_{60}^- ions lose the excess electron by vibrational auto-detachment with a rate constant $k(E_V)$ such that both C_{60}^- ions and C_{60}^0 neutrals are hitting the surface. Their relative fraction for a given nozzle temperature is determined by the decay kinetics. Since the hyperthermal negative ion formation yield is insensitive to the incident charge state one can write for the total scattered C_{60}^- signal:

$$I_{\Sigma}^- \propto \beta^- \cdot I_o \tag{3}$$

where β^- is the probability for incident C_{60}^0 or C_{60}^- to leave the surface as C_{60}^- (i.e. surface electron pickup probability along the outgoing trajectory). The neutral C_{60}^0 flux under the "deflector ON" condition is proportional to $I_o[1-\exp(-k(E_V)\tau)]$. For the intensity I_n^- of scattered C_{60}^- that originated from a pure C_{60}^0 incident beam one can write:

$$I_n^- \propto \beta^- I_o[1 - \exp(-k(E_V)\tau)] \tag{4}$$

Besides charge insensitivity, the use of the same β^- value for both Eq. (3) and (4) is also based on the

relative insensitivity observed for the small differences in vibrational energies between the impinging C_{60}^- and C_{60}^0 (as was discussed in Sec. 2).

The ratio $\alpha(T) = I_n^-/I_\Sigma^-$ is therefore given by:

$$\alpha(T) = 1 - \exp[-k(E_V)\tau]; \quad (5)$$

such that

$$k(E_V(T)) = -\frac{1}{\tau}\ln[1 - \alpha(T)] \quad (6)$$

In order to change from $E_V(T)$ to E_V (T_V) as in Eq. (2) one needs the exact value of $\langle E_e\rangle$ (which is roughly in the range of $\langle E_e\rangle = 0$–2 eV). As a zero order approximation we can assume $\langle E_e\rangle = 0$ and use a thermal rate constant of the form $k(T_V) = A\exp(-E_a/KT_V)$ with K as the Boltzmann constant and E_a the activation energy. Using the measured $\alpha(T)$ values as given in Fig. 5 we get in this case a straight Arrhenius plot [$\ln(k(T_V)$ versus $1/T_V$] with a slope of $E_a = (2.42 \pm 0.06$ eV) and intersection $A = (3.5 \pm 0.2) \times 10^{10}$ s^{-1}. The E_a value obtained shows that the assumption of $\langle E_e\rangle = 0$ is reasonable but not fully justified. However, we can also try a different approach. In principle, one can extract $\langle E_e\rangle$ directly from the experimental measurements using the electron emission kinetics as a vibrational thermometer (T_V) for *one or two nozzle temperatures* (out of six temperatures in Fig. 5) and then use this $\langle E_e\rangle$ value for calculating T_V and plotting Arrhenius plots for *all the temperatures*. To this purpose, we will first develop the proper expression for obtaining T_V (and therefore $\langle E_e\rangle$) for a given nozzle temperature T. From Eq. (6), we can write for the ratio of rate constants between two different nozzle temperatures:

$$\frac{k(T_{V2})}{k(T_{V1})} = \frac{\ln(1 - \alpha(T_{V2}))}{\ln(1 - \alpha(T_{V1}))} \equiv B_{21} \quad (7)$$

Using the thermal decay expression $k(T_V) = A\exp(-\mathrm{EA}/KT_V)$ and the relations $T_{V2} = T_{V1}[1 + (T_{V2} - T_{V1})/T_{V1}]$ and $T_{V1} - T_{V2} = T_1 - T_2$ one finally gets:

$$\ln B_{21} = -\frac{\mathrm{EA}}{K(T_1 - T_2)}\left(\frac{T_1 - T_2}{T_{V1}}\right)^2 \times \left(1 - \frac{T_1 - T_2}{T_{V1}}\right)^{-1} \quad (8)$$

Eq. (8) can be used to determine T_{V1} by measuring T_1 [and $\alpha(T_1)$] and any other arbitrary nozzle temperature T_2 (with its respective $\alpha(T_2)$ value). Note that only temperature differences $(T_1 - T_2)$ need to be accurately measured. A critical test as to the validity and self consistency of this method will be to obtain the same T_{V1} value for several different T_2 [and $\alpha(T_2)$] values.

We first applied this method to the lowest nozzle temperature ($T_1 = 1459$ K) as given in Fig. 5. We repeated the calculation for T_{V1} with all the nozzle temperatures in Fig. 5 excluding the one next to T_1 to avoid large errors associated with measurement of a small temperature difference. For each of the repeated calculations we obtained a rather similar T_{V1} value. This confirms the validity of the analysis. Please note that using *all* the higher temperatures is only for the purpose of verification. The final average value is $T_{V1} = 1741 \pm 22$ K, which corresponds to $E_V = 17.55 \pm 0.31$ eV, according to the $E_V(T_V)$ relation given before. Since $T_1 = 1459$ K corresponds to $\langle E_{\mathrm{th}}(T)\rangle = 13.61$ eV we get $\langle E_e\rangle = E_V - \langle E_{\mathrm{th}}(T)\rangle - \mathrm{EA} = 1.29$ eV. We have also calculated the vibrational temperature for $T = 1539$ K and have used as the reference (second) temperature all the T values above it. This time we have obtained $\langle E_e\rangle = 1.05$ eV. Taking the average of both measurements and considering uncertainties in the T_V values we get a final determination of $\langle E_e\rangle = 1.2 \pm 0.4$ eV. We can now convert all the measured nozzle temperatures as given in Fig. 5 to the corresponding vibrational temperatures using Eq. (2) (with EA = 2.65 eV and $\langle E_e\rangle = 1.2$ eV) and the E_V (T_V) relation. The rate constants $k(T_V)$ are taken from Fig. 5 using Eq. (6) as before. The Arrhenius plot for the new set of corrected vibrational temperatures is shown in Fig. 6. The slope is 2.64 ± 0.07 eV, which is practically identical to the reported EA value. The pre-exponential factor (intersection) is $A = (1.3 \pm 0.1) \times 10^{11}$ s^{-1}. The slope extracted from the Arrhenius plot cannot be considered fully independent since the EA(C_{60}) value served as an input in calculating the vibrational temperatures T_V. It should rather be viewed as a proof for self consistency of the analysis and the derived results. However, $\langle E_e\rangle$ and the pre-

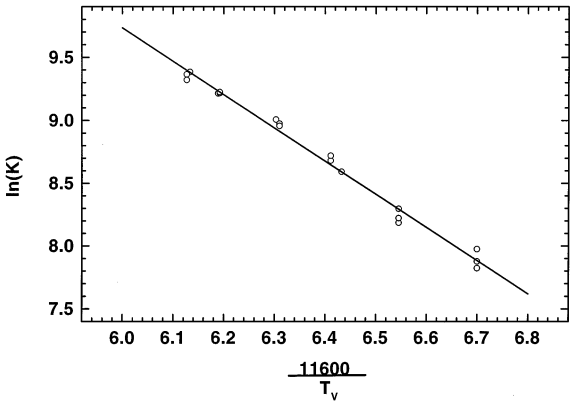

Fig. 6. Arrhenius plot for the thermal auto-detachment process of electrons from C_{60}^- along the flight time τ. The plot is based on the data presented in Fig. 5. The temperature T_V is the vibrational temperature of C_{60}^- as given by Eq. (2) and the rate constant k is related to the flux normalized C_{60}^0 fraction (α) via Eq. (6). The slope of the straight line (best fit) is 2.64 ± 0.07 eV and the intersection with the ln(k) axis is $A = (1.3 \pm 0.1) \times 10^{11}$ s^{-1}.

exponential factor A are uniquely determined by this procedure. The pre-exponential factor obtained is in good agreement with the formerly reported experimental value [6] but is several orders of magnitude lower than predicted by simple thermionic emission models. The predicted value according to the Richardson–Dushman equation [15] (thermal electron emission from solids) for C_{60}^- is 8.0×10^{13} s^{-1}. We have assumed a C_{60}^- diameter of 10 Å and vibrational temperature of 1850 K. If we take into account a degeneracy factor of 6 (t_{1u} orbital) for the excess electron this value will be reduced to 1.6×10^{13} s^{-1} [7]—still a factor of 100 higher than the measured value. The A value predicted according to the thermionic emission model for (neutral) clusters [14a] is even 4–5 orders of magnitude higher then the one measured here for the negative ion. We would like to suggest a tentative explanation for this difference.

The pre-exponential factor stands for the highest rate constant possible for the system and therefore sets the characteristic time scale for the rate-determining step. For delayed electron emission from the superhot neutral C_{60}^0 we have found that the predicted high value of 1.5×10^{16} s^{-1} [14] is in agreement with the experimental results [36]. This implies a rather efficient coupling between the nuclear vibrations and the valence electrons in the neutral molecule. The low A value for the negative ion probably reflects a much weaker coupling (i.e. lower collision rate) between the equilibrated nuclear-electronic system of the neutral C_{60}^0 core and the more distant excess electron. This coupling (i.e. low collision rate bottleneck) can be described in terms of a relatively poor overlap between wave functions tails of the highest occupied molecular orbital (HOMO) electrons of C_{60}^0 and the excess electron in C_{60}^-. This picture is a modification of the simple notion of electronic nuclear equilibration in thermionic emission. We basically suggest that whereas the thermionic (valence) electrons emitted from C_{60}^0 are strongly coupled to the molecular vibrations, the excess (emitted) electron in C_{60}^- does not interact directly with the nuclear system but via a weaker electron–electron coupling with the valence electrons. The delayed electron emission process in this case will still behave thermally but the maximum rate value (A) will be relatively low, as is experimentally observed.

4. Summary

We have studied the thermally activated decay processes of an ensemble of isolated superhot C_{60}^- negative ions in effusive molecular beam. We have applied an innovative charge insensitive detection method for measuring the integrated flux of beams with different charge state compositions. It is based on surface-molecule electron transfer and negative ion formation during hyperthermal scattering. Our conclusions with regard to the main issues of this study as raised in the introduction are as follows: (1) Thermal rate constants (Arrhenius type) provide an excellent description of the delayed electron emission process (vibrational auto-detachment) for a thermally pumped (canonical at the instant of ion formation) ensemble of C_{60}^- ions. (2) A weak dissociative attachment channel $C_{60}^0 + e^- \rightarrow C_{58}^0 + C_2^-$ was observed. This channel was found to be about a factor of 100 slower than the auto-detachment channel. This ratio is in agreement with the estimated energy threshold for the dissociative attachment reaction based on former measure-

ments of superhot C_{60}^0 fragmentation ($C_{60}^0 \rightarrow C_{58}^0 + C_2^0$). (3) No experimental evidence was found for the nearly isoenergetic complementary dissociative attachment channel $C_{60}^0 + e^- \rightarrow C_{58}^- + C_2^0$. This rather surprising result can be explained by assuming that the fragmentation process is very slow (adiabatic) and thus sensitive to small differences of 0.1–0.2 eV (within experimental error) in the electron affinity values of the departing fragments. (4) The low value of the pre-exponential factor measured here ($A = 1.3 \times 10^{11}$ s^{-1}) is in good agreement with the value measured before [6]. This shows that current models whose predictions are several orders of magnitude higher should be revised.

Acknowledgements

This research was supported by a grant from the Israel Science Foundation, a grant from the US–Israel Binational Science Foundation, and in part by the James Franck program and the fund for promotion of research at the Technion.

References

[1] O. Ingolfsson, F. Weik, E. Illenberger, Int. J. Mass Spectrom Ion Processes 155 (1996) 1 (review, with references therein).
[2] L.G. Christophorou, in Advances in Electronics and Electron Physics, Academic, New York, 1978, Vol. 46, p. 55.
[3] S. Tobita, M. Meinke, E. Illenberger, L.G. Christophorou, H. Baumgärtel, S. Leach, Chem. Phys. 161 (1992) 501.
[4] M. Lezius, P. Scheier, T.D. Märk, Chem. Phys. Lett. 203 (1993) 232.
[5] T. Jaffke, E. Illenberger, M. Lezius, S. Matejcik, D. Smith, T.D. Märk, Chem. Phys. Lett. 226 (1994) 213.
[6] S. Matejcik, T.D. Märk, P. Spanel, D. Smith, T. Jaffke, E. Illenberger, J. Chem. Phys. 102 (1995) 2516.
[7] J.U. Andersen, C. Brink, D. Hvelplund, M.O. Larsson, B.B. Nielsen, H. Shen, Phys. Rev. Lett. 77 (1996) 3991.
[8] J. Huang, H.S. Caraman Jr., R.N. Compton, J. Phys. Chem 99 (1995) 1719.
[9] C. Yeretzian, K. Hansen, R.L. Whetten, Science 260 (1993) 652.
[10] D. Smith, P. Spanel, J. Phys. B 29 (1996) 5199.
[11] O. Elhamidi, J. Pommier, R. Abouaf, J. Phys. B 30 (1997) 4633.
[12] A. Bekkerman, B. Tsipinyuk, A. Budrevich, E. Kolodney, J. Chem. Phys. 108 (1998) 5165.
[13] L.S. Wang, J. Conceicao, C. Jim, R.E. Smalley, Chem. Phys. Lett. 182 (1991) 5.
[14] (a) C.E. Klots, Chem. Phys. Lett. 186 (1991) 73; (b) C.E. Klots, R.N. Compton, Surf. Rev. Lett. 3 (1996) 535.
[15] N.W. Aschroff, N.D. Mermin, in Solid State Physics, Holt–Saunders International Editions, New York, 1976.
[16] K.M. Ervin, W.C. Lineberger, J. Phys. Chem. 95 (1991) 1167.
[17] S.H. Yang, C.L. Pettiette, J. Conceicao, O. Cheshnovsky, R.E. Smalley, Chem. Phys. Lett. 233 (1987) 233.
[18] E. Kolodney, B. Tsipinyuk, A. Budrevich, J. Chem. Phys. 102 (1995) 9263.
[19] E. Kolodney, B. Tsipinyuk, A. Bekkerman, Fullerene Sci. Technol. 6 (1998) 67.
[20] E. Kolodney, B. Tsipinyuk, A. Budrevich, J. Chem. Phys. 100 (1994) 8542.
[21] (a) A. Bekkerman, B. Tsipinyuk, S. Verkhoturov, E. Kolodney, J. Chem. Phys. 109 (1998) 86520; (b) A. Bekkerman, B. Tsipinyuk, E. Kolodney, J. Chem. Phys. (unpublished).
[22] A. Danon, A. Amirav, J. Phys. Chem. 93 (1989) 5549.
[23] A. Danon, E. Kolodney, A. Amirav, Surf. Sci. 193 (1988) 132.
[24] J. Los, J.J.C. Geerlins, Phys. Rep. 190 (1990) 133 (review, with references therein).
[25] P.H.F. Reijner, A.W. Kleyn, Chem. Phys. 139 (1989) 489.
[26] B. Tsipinyuk, A. Budrevich, M. Grinberg, E. Kolodney, J. Chem. Phys. 106 (1997) 2449.
[27] A. Bekkerman, B. Tsipinyuk, A. Budrevich, E. Kolodney, Int. J. Mass Spectrom. Ion Processes 167/168 (1997) 559.
[28] E. Kolodney, B. Tsipinyuk, A. Bekkerman, A. Budrevich, Nucl. Instrum. Methods B 125 (1997) 170.
[29] R. Wörgötter, B. Dünsor, P. Scheier, T.D. Märk, M. Foltin, C.E. Klots, J. Laskin, C. Lifshitz, J. Chem. Phys. 104 (1996) 1225.
[30] A. Budrevich, B. Tsipinyuk, A. Bekkerman, E. Kolodney, J. Chem. Phys. 106 (1997) 5771.
[31] E. Kolodney, B. Tsipinyuk, A. Budrevich, Phys. Rev. Lett. 74 (1995) 510.
[32] P.L. Jones, R.D. Mead, B.E. Kohler, S.D. Rosner, W.C. Lineberger, J. Chem. Phys. 73 (1980) 4419.
[33] S. Yang, K.J. Tayler, M.J. Craycraft, J. Conceicao, C.L. Pettiette, O. Cheshnovsky, R.E. Smalley, Chem. Phys. Lett. 144 (1988) 431.
[34] P.P. Radi, M.T. Hsu, M.E. Rincon, P.P. Kemper, M.T. Bowers, Chem. Phys. Lett. 174 (1190) 223.
[35] P. Sandler, C. Lifshitz, C.E. Klots, Chem. Phys. Lett. 200 (1992) 445.
[36] The measurements and simulation of delayed electron emission from C_{60}^0 are described in [12]. We would like to correct a print error in the A value appearing there. The correct value that was used in the simulation in [12] is $A_i = 8.41 \times 10^{12}$ s^{-1}. For $T_V = 1800$ K we obtain $A = A_i T_V = 1.5 \times 10^{16}$ s^{-1}.